

Critical Casimir interaction of ellipsoidal colloids with a planar wall

S. Kondrat, L. Harnau, and S. Dietrich

*Max-Planck-Institut für Metallforschung, Heisenbergstr. 3, D-70569 Stuttgart, Germany and
Institut für Theoretische und Angewandte Physik,*

Universität Stuttgart, Pfaffenwaldring 57, D-70569 Stuttgart, Germany

(Dated: October 30, 2018)

Based on renormalization group concepts and explicit mean field calculations we study the universal contribution to the effective force and torque acting on an ellipsoidal colloidal particle which is dissolved in a critical fluid and is close to a homogeneous planar substrate. At the same closest distance between the substrate and the surface of the particle, the ellipsoidal particle prefers an orientation parallel to the substrate and the magnitude of the fluctuation induced force is larger than if the orientation of the particle is perpendicular to the substrate. The sign of the critical torque acting on the ellipsoidal particle depends on the type of boundary conditions for the order parameter at the particle and substrate surfaces, and on the pivot with respect to which the particle rotates.

I. INTRODUCTION

The confinement of the order parameter fluctuations in a critical fluid leads to an effective long-ranged interaction between the confining walls and colloidal particles suspended in the fluid. The occurrence of such a force was predicted by Fisher and de Gennes in 1978 [1]. It is called critical (or thermodynamic) Casimir force [2, 3], in analogy with the Casimir force [4] in quantum electrodynamics where the force originates from the confined quantum fluctuations of the electromagnetic field [5].

Since then the critical Casimir effect has attracted increasing theoretical and experimental attention. So far the theoretical investigations of the critical Casimir effect have been focused on the film geometry, realized either by homogeneous, planar, and parallel walls (see, e.g., Refs. [6, 7, 8, 9, 10, 11, 12, 13, 14, 15, 16, 17] and references therein) or by chemically patterned [18] or geometrically structured substrates [19], as well as on spherical colloidal particles (see, e.g., Refs. [20, 21, 22, 23] and references therein). Strong experimental evidences for critical Casimir forces have been obtained by studying wetting films near critical end points of quantum [24, 25, 26] or classical fluids [27, 28].

It has been pointed out by Fisher and de Gennes [1, 29] that such fluctuation-induced forces should lead to flocculation of colloidal particles if their solvent is a binary liquid mixture close to its consolute point. Such a solvent-mediated flocculation, which can be interpreted as indirect evidence for the critical Casimir force, has indeed been observed for silica spheres suspended in a binary liquid mixture of water and lutidine [30, 31, 32, 33] (see also Ref. [34] and references therein) as well as in other binary mixtures [35, 36, 37, 38]. However, only recently, the first *direct* experimental evidence of the critical Casimir force has been reported concerning the force between a spherical colloidal particle and a homogeneous [39] or chemically patterned [40, 41] wall.

In the present study we analyze the critical Casimir effect for non-spherical colloidal particles. In this case, there is not only a force acting between particles or be-

tween a particle and a wall but there is also a *torque* exerted on the particle. This may lead to interesting effects such as orientational ordering of non-spherical colloids in a critical solvent or anchoring of non-spherical particles at a wall. By varying the temperature the strength of this orientational interaction can be tuned and by changing chemically the preferences of the surfaces for the two species forming the solvent one can choose the sign of the interaction [18, 40, 41]. Motivated by this prospect we therefore extend our previous study of critical adsorption at a single non-spherical colloidal particle [42] to the case that in addition there is a planar wall present.

This kind of orientation dependence of fluctuation-induced forces has recently been studied for quantum mechanical Casimir forces [43, 44]. As far as torque due to critical fluctuations is concerned, in Ref. [45] the critical Casimir torque on the confining walls of a wedge has been analyzed. Based on field-theoretic techniques the interaction of non-spherical particles, embedded into a solution of long polymers, with a planar wall has been investigated in the limiting case that the size of the particle is much smaller than the distance from the wall (“protein limit”) and which, in turn, is assumed to be much smaller than the correlation length [46, 47, 48, 49]. These latter analyses show, in particular, that for a solution of ideal polymer chains the preferred orientation of the elongated colloidal particle changes from being perpendicular to being parallel to the substrate surface upon decreasing the particle-wall distance [46, 47], whereas in a solvent of self-avoiding chains the preferred orientation is the parallel one for all distances [49].

The theoretical interest in the behavior of non-spherical colloidal particles is matched by an increased experimental interest, even with application perspectives [50]. Rodlike [51] or disklike [52] architectures, dumbbell-shaped particles [53, 54], and particles with ellipsoidal shape [55, 56] have been synthesized and characterized. The size of these particles ranges between 10 nm and 10 μm . Very recently the influence of an effective torque exerted by a non-critical one-component solvent on dumbbell-shaped particles has been revealed using de-

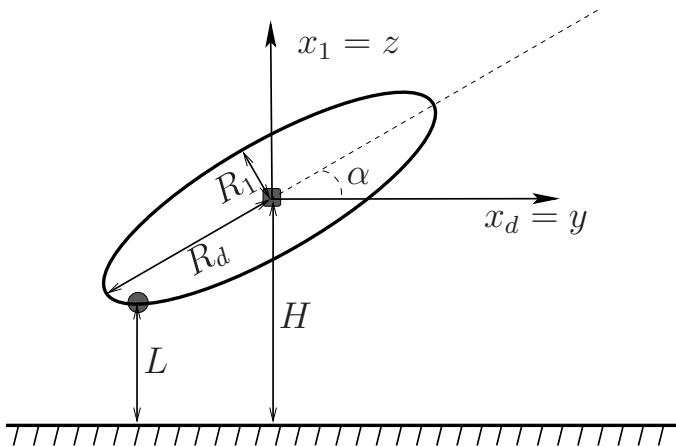


FIG. 1: Schematic side view of an ellipsoid near a planar wall. The ellipsoid semi-axes are $R \equiv R_1 \leq R_2 \leq \dots \leq R_d$. Only the projection onto the $(x_1, x_d) \equiv (y, z)$ plane is shown. The angle between the long axis of the ellipsoid and the wall surface is denoted as α , and the closest distance between the wall and the surface of the ellipsoid is denoted as L , while the distance between the center of the ellipsoid and the wall is denoted as H . The full circle and the square denote two pivots which we use to calculate the torque (see Subsec. III C).

polarized light scattering [57]. For this system, it has been demonstrated that the addition of small amounts of electrolyte has a significant impact on the rotational motion and the aggregation stability of these non-spherical particles, while changes of the temperature typically result in only minor changes of the effective interaction between colloidal particles because this solvent is not close to a continuous phase transition. However, as stated above, near a critical point the effective interaction is expected to exhibit a very sensitive temperature dependence.

The remainder of the paper is organized as follows. In Sec. II we define the system under consideration and we introduce the scaling functions for the critical Casimir interactions. In order to calculate the force and the torque we use the stress tensor, as described in Subsec. III A. The results of the full mean field calculations are discussed in Subsecs. III B and III C. In Sec. IV we compare qualitatively the quantum-electrodynamic Casimir, critical Casimir, and polymer depletion interactions acting on an ellipsoidal colloid close to a wall. Finally, in Sec. V we briefly summarize our results.

II. MODEL

In order to be able to discuss and to compare the behavior of both non-spherical as well as spherical colloidal particles, we describe them in a unified way by consider-

ing a particle with the shape of a hypercylinder:

$$\mathcal{K}_d(\{R_i\}) = \left\{ \mathbf{r} = (x_1, x_2, \dots, x_D) \right. \\ \left. \left| \sum_{s=1}^d \left(\frac{x_s}{R_s} \right)^2 \leq 1, \quad d \leq D \right\}, \quad (1)$$

where $R = R_1 \leq R_2 \leq \dots \leq R_d$ are the semi-axes of the hypercylinder (see Fig. 1). If $R = R_1 = \dots = R_d$ and $d = D$, the hypercylinder reduces to a hypersphere. If not all semi-axes are equal but $d = D$ the hypercylinder is an ellipsoid. It is called a spheroid if only two semi-axes are different: in $D = 3$ one has a prolate spheroid ($R_1 = R_2 < R_3$) and an oblate spheroid ($R_1 < R_2 = R_3$). In the case $1 < d < D$, we have a spheroidal cylinder (or “spheroido-cylinder”), with a $D - d$ dimensional hyperaxis. For reasons of simplicity, and in order to distinguish the cases of equal and different semi-axes, we shall use the notion of a disk ($d = 2$) and of a d -sphere ($d \geq 3$) if all finite axes are equal (note that they are cylinders for $D > d$), while the case in which some of the axes are different will simply be denoted as an ellipse or as a spheroid (or ellipsoid) depending on d (note that they are spheroido-cylinders in $D > d$).

We consider the generalization of D to values different from three because the upper critical dimension (for the Ising universality class of the fluids discussed here) is $D^* = 4$. We recall that the universal quantities such as critical exponents and universal scaling functions calculated within mean field theory (MFT) are exact in $D > D^*$. (For $D = D^*$ one expects logarithmic corrections which we do not consider here.) Accordingly, our MFT results (see Sec. III) can be interpreted either as exact results in $D > D^*$ or as mean field approximations for the dimensions $D = 3$ or $D = 2$.

The effective force f acting on a particle in the direction normal to the substrate is the negative derivative of the free energy \mathcal{F} of the confined fluid with respect to the closest distance L of the particle from the wall at fixed orientation. Close to a critical point it decomposes into the sum of an analytical background part and of a non-analytical (singular) part [6, 7, 8] (for further details see Ref. [15]). According to the scaling behavior predicted by renormalization group theory the latter (divided by the “length” of the $(D - d)$ -dimensional hyperaxis of the hypercylinder along which \mathcal{K}_d is translational invariant), in the case of an ellipsoidal particle close to the wall, can be cast into the form ($s = 1, \dots, d - 1$) [22]:

$$f(L, R_1, \dots, R_d, \{\alpha_p\}, T) = \frac{k_B T}{L^{D-d+1}} \\ \times K_{\pm} \left(\Theta_{\pm} = L/\xi_{\pm}, \Delta = L/R, \{\alpha_p\}; \right. \\ \left. \{\delta_s = R_{s+1}/R\} \right), \quad (2)$$

where $\{\alpha_p\}$ are $d(d - 1)/2$ angles determining the orientation of the hypercylinder, $\xi_{\pm} = \xi_0^{\pm} |t|^{-\nu}$ is the bulk correlation length in the disordered (+) and ordered (-)

phase, respectively, $t = (T - T_c)/T_c$ with ν as a standard bulk critical exponent, and ξ_0^\pm are non-universal amplitudes. L is the closest distance between the surface of the ellipsoid and the wall (see Fig. 1), $R = R_1$, and K_\pm are dimensionless universal scaling functions. $f > 0$ ($f < 0$) corresponds to repulsive (attractive) forces.

In addition, a non-spherical particle experiences an effective torque, the components of which are, in general, linear combinations of the (negative) derivatives of the free energy with respect to the angles $\{\alpha_p\}$. In the case shown in Fig. 1, the torque has only one non-zero component describing the rotations within the yz plane; this component equals the negative derivative of the free energy \mathcal{F} with respect to the angle α . In general, the non-analytic contribution to the torque per “length” of the $(D - d)$ -dimensional hyperaxis of \mathcal{K}_d takes on the scaling form

$$\mathbf{t}(L, R_1, \dots, R_d, \{\alpha_p\}, T) = \frac{k_B T}{L^{D-d}} \times M_\pm(\Theta_\pm, \Delta, \{\alpha_p\}; \{\delta_s\}), \quad (3)$$

where M_\pm are the universal scaling functions of the torque. We note that \mathbf{t} (and therefore M_\pm) is an antisymmetric tensor of the second rank (the so-called 2-form). In D dimensions \mathbf{t} has, in general, $\binom{D}{p=2} = D!/(2(D-2)!)$ components. However, because of the translational invariance in $(D - d)$ directions, only $\binom{d}{2} = d(d-1)/2$ of them are non-zero (some of them may as well be zero depending on additional symmetries of \mathcal{K}_d). In $D = 3$ dimension the conventional torque pseudo-vector \mathbf{t} is obtained by taking the Hodge dual of \mathbf{t} , i.e., $\mathbf{t} = *\mathbf{t}$; in Euclidian space $\mathbf{t}_k = (1/2!) \sum_{i,j} t_{ij} \epsilon_{ijk}$, where ϵ_{ijk} is the Levi-Civita symbol.

In the literature two common choices are used to define the distance between the particle and the wall: The surface-to-surface distance L (used, e.g., in Refs. [22, 23, 41]) and the distance H from the center of the particle to the wall (used, e.g., in Refs. [44, 46, 47, 48, 49]), see Fig. 1. Correspondingly, one can also define two different pivots (points of rotation) with respect to which the particle rotates: The point on the surface of the particle closest to the wall (denoted by a circle in Fig. 1) in the former case and the center of a particle (denoted by a square in Fig. 1) in the latter case. While it is obvious that the force does not depend on the definition of the distance, the torque does depend on the choice of the pivot. It is easy to see, however, that the values of the torque corresponding to two different pivots, $\mathbf{t}^{(1)}$ and $\mathbf{t}^{(2)}$, are related by the simple equation (see, c.f., also Eq. (16))

$$\mathbf{t}^{(1)} = \mathbf{t}^{(2)} + \mathbf{r}^{(12)} \wedge \mathbf{f}, \quad (4)$$

where $\mathbf{r}^{(12)} = \mathbf{r}^{(1)} - \mathbf{r}^{(2)}$ is the vector connecting the two pivot points located at $\mathbf{r}^{(1)}$ and $\mathbf{r}^{(2)}$, respectively. \mathbf{f} is the vector of the force, and \wedge denotes the wedge product (a multi-dimensional analogue of the three-dimensional cross product; its ij component is given by $(\mathbf{r}^{(12)} \wedge \mathbf{f})_{ij} =$

$x_i^{(12)} f_j - x_j^{(12)} f_i$, where $x_i^{(12)}$ is the i -th component of $\mathbf{r}^{(12)}$. In the following we shall calculate the scaling functions K_\pm and M_\pm within MFT, and we will also compare and discuss in more detail the scaling functions for these two choices of the distance and of the pivot (see Sec. III B and III C).

III. MEAN-FIELD APPROXIMATION

The standard Landau–Ginzburg–Wilson Hamiltonian for critical phenomena confined to a volume V is given by

$$\mathcal{H}[\phi] = \int_V dV \left(\frac{1}{2} (\nabla \phi)^2 + \frac{\tau}{2} \phi^2 + \frac{u}{24} \phi^4 \right) \quad (5)$$

augmented by boundary conditions [58, 59]. In the case of a binary liquid mixture near its consolute point the order parameter ϕ is proportional to the difference of the concentrations of its two species; τ is proportional to t and u is a coupling constant which stabilizes $\mathcal{H}[\phi]$ in the ordered phase. For the critical adsorption fixed point [59], valid for confined fluids, the boundary conditions are $\phi = +\infty$ (or $\phi = -\infty$) at the surface of the colloidal particle and at the wall, to which we refer to in the following as the “+” (or “-”) boundary condition. The semi-axes $\{R_i\}$ of the hypercylinder (see Fig. 1) introduce additional length scales which might come into play via coupling constants of additional surface terms in the effective Hamiltonian [59]. However, on the basis of power counting one concludes that such terms are irrelevant at the ordinary transition (corresponding to the Dirichlet boundary conditions), where the surface enhancement coupling of the term proportional to ϕ^2 at the surface asymptotically dominates $1/R_i$ contributions to couplings of symmetry-preserving boundary terms. On the same footing we expect that the distinctive feature of the normal transition, i.e., the occurrence of symmetry breaking with a resulting asymptotic divergence of the order parameter at the surface is asymptotically not affected by curvatures; curvatures might perhaps influence the cross-over between the ordinary and the normal transitions. Accordingly, we do not expect the aforementioned asymptotic boundary conditions to be modified by curvature.

Within MFT, the fluctuations of the order parameter ϕ are neglected and only the order parameter configuration with the largest statistical weight, $m = \sqrt{u/6} \langle \phi \rangle$, is taken into account. Minimization of Eq. (5) leads to the Euler–Lagrange equation

$$\Delta m = \tau m + m^3. \quad (6)$$

Equation (6) is solved numerically as function of τ using the finite element method (see, e.g., Ref. [60]). We consider only hypercylinders $\mathcal{K}_d(\{R_i\})$ with $d = 2$ and $d = 3$, for which the problem is effectively two- and three-dimensional, respectively (for $\mathcal{K}_{d \geq 4}$ one has a four and

higher dimensional problem which is difficult to solve numerically). For reasons of simplicity we also restrict our considerations to the case of only two different semi-axes, $R = R_1 = \dots = R_{d-1} < R_d$, i.e., we consider a prolate spheroid in spatial dimension d (which is a spheroidocylinder in spatial dimension $D > d$). We expect that the results for an oblate spheroid do not differ qualitatively. In Eq. (6) τ can be expressed in terms of the bulk correlation length ξ_{\pm} , which governs the exponential decay of the two-point correlation function in the bulk: $\tau = \xi_+^{-2}$ for $\tau > 0$ and $\tau = -\xi_-^{-2}/2$ for $\tau < 0$.

We note that the contribution from the square gradient term in Eq. (5) does not vanish in the case of the ellipsoid-wall geometry with symmetry-breaking boundary conditions. Therefore, one does not expect an additional thermodynamic length [61] to emerge and to affect finite-size scaling in dimensions $D > D^*$. Such a thermodynamic length naturally emerges in the finite-size scaling analysis for $D > D^*$ if the standard mean-field theory in a finite volume exhibits an isolated zero mode which becomes “massless” at the bulk critical point due to the absence of a nonvanishing contribution from the square gradient term in Eq. (5).

A. The stress tensor

By using the stress tensor, the force and the torque can be calculated directly from the order parameter profile $m(\mathbf{r})$. This has the advantage that one avoids the numerical difficulties of calculating differences of free energies which attain large values due to the divergence of the order parameter profile at the surfaces.

We consider an infinitesimal, local coordinate transformation ($k = 1, \dots, D$):

$$x'_k = x_k + \sum_j X_{kj} \delta\omega_j(\mathbf{r}), \quad (7)$$

where the meaning of the index j depends on the kind of transformation and is specified below. The linear response of a system to such a coordinate transformation is

$$\delta\mathcal{H} = \int_V dV \sum_{j,k} \theta_{jk}(\mathbf{r}) \frac{\partial \delta\omega_j}{\partial x_k}, \quad (8)$$

where $(\partial_n m = \partial m / \partial x_n)$

$$\theta_{jk}(\mathbf{r}) = \frac{\partial \mathcal{L}}{\partial (\partial_k m)} \sum_n (\partial_n m) X_{jn} - \mathcal{L} X_{jk}. \quad (9)$$

In Eq. (9) $\mathcal{L}(m, \partial m)$ is the integrand of the Hamiltonian \mathcal{H} given by Eq. (5). In order to calculate the force, we use the coordinate transformation with $X_{jk} = \delta_{jk}$ ($j, k = 1, \dots, D$) and $\delta\omega_z(\mathbf{r}) = a$ for $\mathbf{r} \in V_0$ and $\delta\omega_k(\mathbf{r}) = 0$ otherwise, where V_0 is a generalized hypercylinder enclosing \mathcal{K}_d . Accordingly, the z -component of the force, which is the only non-zero component (see

Fig. 1), divided by the “length” $\ell = \int d^{D-d}x$ of the $(D-d)$ -dimensional hyperaxis of \mathcal{K}_d is given by [23]

$$\frac{f}{k_B T} = -\frac{1}{\ell} \frac{\partial \delta\mathcal{H}}{\partial a} = \frac{1}{\ell} \oint_S dS \sum_{k=1}^D \mathcal{T}_{zk} \hat{n}_k = -\frac{1}{\ell} \frac{\partial \mathcal{F}}{\partial L}, \quad (10)$$

where within MFT $\mathcal{F} = \min_{\phi} (\mathcal{H}[\phi])$. S denotes the surface of V_0 , \hat{n}_k is the k -th component of its unit outward normal, $dS = d^{D-1}x$, and \mathcal{T}_{jk} is the conventional stress tensor:

$$\mathcal{T}_{jk} = \frac{\delta \mathcal{L}}{\delta (\partial_k m)} \partial_j m - \delta_{jk} \mathcal{L}. \quad (11)$$

One often adds to \mathcal{T} the so-called “improvement” term (see, e.g., Refs. [13, 14, 18, 23]),

$$\mathcal{I}_{kl} = \frac{1}{4} \frac{D-2}{D-1} [\partial_k \partial_l - \delta_{kl} \Delta] m^2, \quad (12)$$

which ensures the scale and conformal invariance of the stress tensor at the critical point and renders it renormalizable [62, 63, 64, 65]. However, the contributions from this term to ‘observable quantities’ like the force or the torque vanish. For instance, in the case of the force one obtains with the help of the Gauss-Ostrogradsky theorem (using here the summation convention) $\oint_S \mathcal{I}_{lk} \hat{n}_l dS = \int_{V_0} \partial_l \mathcal{I}_{lk} dV \equiv 0$ because $\partial_l \mathcal{I}_{lk} = 0$.

In order to calculate the torque, the coordinate transformation (7) is chosen to take the form of an infinitesimal rotation, i.e.,

$$x'_k = x_k + \sum_{\substack{n=1 \\ n \neq k}}^D x_n \delta\omega_{nk} = x_k + \sum_{\substack{l,n=1 \\ n < l}}^D X_{k,nl} \delta\omega_{nl}, \quad (13)$$

where $X_{k,nl} = x_l \delta_{kn} - x_n \delta_{kl}$ and the antisymmetry of $\delta\omega_{nk}$ has been used. Note that here the index j in Eq. (7) consists of two indices, $j \rightarrow (nl)$, which denote the rotation plane. Now we choose $\delta\omega_{yz}(\mathbf{r}) = \alpha$ for $\mathbf{r} \in V_0$ and $\delta\omega_{nk}(\mathbf{r}) = 0$ otherwise (see Fig. 1). This renders the (only non-zero) component of the torque (per “length” of the $(D-d)$ -dimensional hyperaxis of \mathcal{K}_d):

$$\frac{\tau_{yz}}{k_B T} = -\frac{1}{\ell} \frac{\partial \delta\mathcal{H}}{\partial \alpha} = \frac{1}{\ell} \oint_S dS \sum_{k=1}^D \mathcal{M}_{k,yz} \hat{n}_k = -\frac{1}{\ell} \frac{\partial \mathcal{F}}{\partial \alpha}, \quad (14)$$

where the “angular momentum” tensor $\mathcal{M}_{k,nl}$ is

$$\mathcal{M}_{k,nl} = (x_l - x_l^{(1)}) \mathcal{T}_{kn} - (x_n - x_n^{(1)}) \mathcal{T}_{kl}, \quad (15)$$

with $x_l^{(1)}$ being the l component of the position vector of the pivot with respect to which the ellipsoid rotates. If we choose $x_l^{(1)} = x_l^{(2)} + x_l^{(12)}$, where $x_l^{(2)}$ is the l component of the position vector of another pivot and $x_l^{(12)}$ is the l

component of the vector $\mathbf{r}^{(12)} = \mathbf{r}^{(1)} - \mathbf{r}^{(2)}$ connecting the two pivots, then by using Eqs. (10) and (14) we obtain

$$\mathbf{t}_{nl}^{(1)} = \mathbf{t}_{nl}^{(2)} + x_n^{(12)} f_l - x_l^{(12)} f_n, \quad (16)$$

where f_l is the l component of the force \mathbf{f} (we recall that in our case only $f_z \equiv f \neq 0$), and $\mathbf{t}_{nl}^{(i)}$ denotes the (nl) component of the torque corresponding to the i -th pivot. Equation (16) is the component version of Eq. (4).

B. Casimir force

We first study the influence of the anisotropy of the particle on the Casimir force for $D = 4$. In Fig. 2(b) we compare the universal scaling functions K_{\pm} , as functions of the rescaled distance $\Theta_{\pm} = L/\xi_{\pm}$, for a spheroidal particle $\mathcal{K}_{d=3}$ and for two ($d = 3$)-spheres (see Eq. (1)) in the case of ++ boundary conditions which lead to attractive forces. In particular, we compare the two extreme orientations $\alpha = 0$ and $\alpha = \pi/2$ of a spheroid (i.e., the particle is oriented parallel and perpendicular to the wall, respectively, see Fig. 1) with two ($d = 3$)-spheres: a small one with its radius equal to the smallest semi-axis ($R = R_1$), and a bigger one with its radius equal to the major semi-axis of the spheroid ($R = R_d = 2R_1$). It is interesting that the force is stronger for the small sphere ((2) in Fig. 2(a)) than for the spheroid oriented perpendicular to the wall ((1) in Fig. 2(a)). Indeed, within the Derjaguin approximation [66, 67] the force is inversely proportional to the square root of the Gaussian curvature $G = \kappa^{(1)}\kappa^{(2)}$ of the particle surface at the point closest to the wall (c.f., Eq. (17)); $\kappa^{(i)}$ are the principle curvatures. The square root of the Gaussian curvature of the sphere is $G_{\text{sphere}}^{1/2} = 1/R_1$ while the principle curvatures of the spheroid at its elongated edge ($\alpha = \pi/2$) are $\kappa_{\text{spheroid}}^{(1)} = \kappa_{\text{spheroid}}^{(2)} = R_d/R_1^2$ so that $G_{\text{spheroid}}^{1/2}(\alpha = \pi/2) = R_d/R_1^2$, which is larger than $G_{\text{sphere}}^{1/2}$ if $R_d > R_1$ (which is the present case, see Fig. 2(a)). For $\alpha = 0$ ((3) in Fig. 2(a)) one has $G_{\text{spheroid}}^{1/2}(\alpha = \pi/2) = 1/R_d$ which equals $G_{\text{sphere}}^{1/2} = 1/R_d$ for (4) in Fig. 2(a). Thus the configurations (3) and (4) in Fig. 2(a) have the same Gaussian curvature at the point closest to the wall so that within the Derjaguin approximation given by, c.f., Eq. (17) both cases lead to the same critical Casimir force. Therefore the difference between the curves (3) and (4) in Fig. 2(b) highlights the shortcomings of the Derjaguin approximation (Eq. (17)) for this geometrical set-up. The scaling functions for intermediate orientations and for ++ as well as +- boundary conditions are shown in Fig. 3. The minima of the scaling functions for ++ boundary conditions occur at $T > T_c$. They move closer to T_c upon changing the orientation of the particle from parallel to perpendicular.

It is instructive to compare our full MFT results with the Derjaguin (or proximity force) approximation

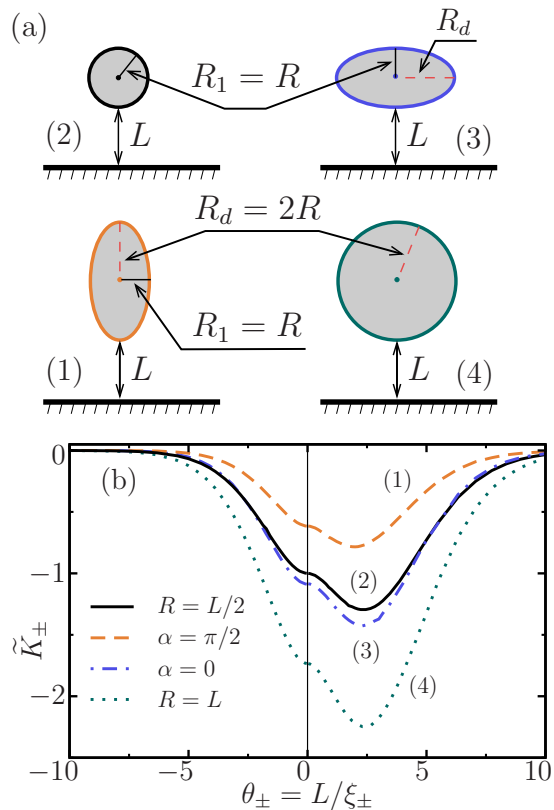


FIG. 2: (color online) (a) Two spheres ((2) and (4)) and one spheroid with perpendicular ($\alpha = \pi/2$; (1)) and parallel ($\alpha = 0$; (3)) orientation at the same surface-to-surface distance L from the wall. (b) The universal scaling functions $\tilde{K}_{\pm} = K_{\pm}(\Theta_{\pm}, \Delta = 2, \alpha; \delta = 2)/|K_{\pm}(\Theta_{\pm} = 0, \Delta = 2; \delta = 1)|$ as a function of the rescaled reduced temperature $\Theta_{\pm} = L/\xi_{\pm} = |t|^{\nu} L/\xi_0^{\pm}$, where $\delta = R_d/R$. The curves (2) and (4) correspond to ($d = 3$)-spheres with radii $R = R_1 = L/2$ and $R = R_d = 2R_1 = L$, respectively. The curves (1) and (3) correspond to a prolate spheroid with $R = R_1 = R_2 < R_{d=3}$ (spheroidocylinder \mathcal{K}_3 in spatial dimension $D \geq 4$) for $\Delta = L/R = 2$, $\delta = R_{d=3}/R = 2$, and the orientations $\alpha = \pi/2$ and $\alpha = 0$, respectively, where α is the angle between the main axis of the spheroid and the wall (see Fig. 1). In all cases ++ boundary conditions are imposed. The force is expressed in units of the absolute value of the Casimir force for the sphere with radius $R = L/2$ at the critical point ($\Theta_{+} = 0$) and for ++ boundary conditions (accordingly, at $\Theta_{+} = 0$ line (2) is normalized to -1).

[66, 67], which is applicable for large particles close to the wall. In lowest order in curvatures one obtains

$$K_{\pm}(\Theta, \Delta, \alpha; \delta) = \frac{(2\pi)^{(d-1)/2}}{\Gamma((d+1)/2)} \tilde{G}^{-1/2}(\Delta, \delta, \alpha) \times \int_1^{\infty} \frac{K_{\pm}^{(||)}(\Theta u)}{u^D} (u-1)^{(d-3)/2} du, \quad (17)$$

where $K_{\pm}^{(||)}$ is the scaling function for the plate-plate geometry, $\Gamma(x)$ is the Gamma function, and $\tilde{G}(\Delta, \delta, \alpha) =$

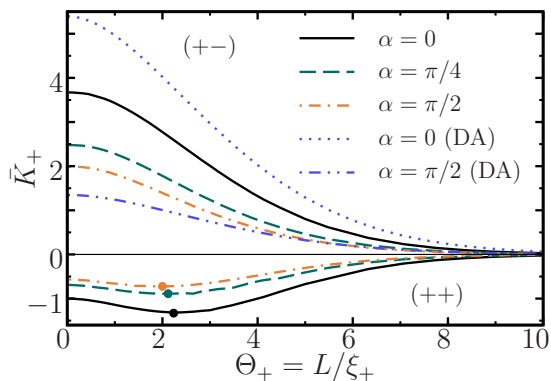


FIG. 3: (color online) The universal scaling function $\bar{K}_+ = K_+(\Theta_+, \Delta = 2, \alpha; \delta = 2)/|K_+(\Theta_+ = 0, \Delta = 2, \alpha = 0; \delta = 2)|$ as a function of the rescaled reduced temperature $\Theta_+ = L/\xi_+ = t^\nu L/\xi_0^+$ for a prolate spheroid $R = R_1 = R_2 < R_3$ (spheroido-cylinder $\mathcal{K}_{d=3}$ in $D > d$) for $\Delta = L/R = 2$ and $\delta = R_3/R = 2$, and for three values of the angle α between the main axis of the spheroid and the wall (see Fig. 1). The positive (negative) curves correspond to $+ -$ ($++$) boundary conditions on the spheroid and the wall leading to repulsion (attraction). The force is expressed in units of the absolute value of the Casimir force for $\alpha = 0$ at the critical point ($\Theta_+ = 0$) and for $++$ boundary conditions. Accordingly, at $\Theta_+ = 0$ the bottom curve is normalized to -1 . (Note that here the normalization differs from the one used in Fig. 2.) The dots denote the minima of the scaling function. Dotted and dash-double dotted lines show the Derjaguin approximation (DA) for $\alpha = 0$ and $\alpha = \pi/2$, respectively, and for $+ -$ boundary conditions. According to Eqs. (17) and (18) these two curves differ only by an overall scale factor $\delta^2 = 4$.

$L^{d-1} \prod_{s=1}^{d-1} \kappa^{(s)}$ (where $\kappa^{(s)}$ are the principle curvatures) is the dimensionless Gaussian curvature of the particle surface at the point closest to the wall. In the case of the spheroid $\mathcal{K}_{d=3}$ one has

$$\tilde{G}(\Delta, \delta, \varphi(\alpha)) = \frac{\Delta^2 \delta^2}{(1 + (\delta^2 - 1) \cos^2 \varphi(\alpha))^2}, \quad (18)$$

where φ is the parametric latitude denoting the position on the spheroid surface parameterized as $(R_1 \cos \varphi \cos \psi, R_1 \cos \varphi \sin \psi, R_d \sin \varphi)$ with ψ as the longitude. The value of φ at the point closest to the wall depends on α ; $\varphi(\alpha = 0) = 0$ and $\varphi(\alpha = \pi/2) = \pi/2$.

The results within the Derjaguin approximation (using the mean field scaling function $K_{\pm}^{(ll)}$) are shown in Fig. 3 by dotted and dash-double dotted lines. In order to avoid overloading Fig. 3, the Derjaguin results are presented only for two angles, $\alpha = 0$ and $\alpha = \pi/2$. For these two angles the Derjaguin results differ only by an overall scale factor δ^2 with $\delta^2 = 4$ here. For both angles the discrepancy with the full mean field results is rather large. The reason is that in the case studied here the ratio $\Delta = L/R = 2$, while the Derjaguin approximation is supposed to be valid in the limit of small distances (or big particles), i.e., for $\Delta \rightarrow 0$. It is interesting to

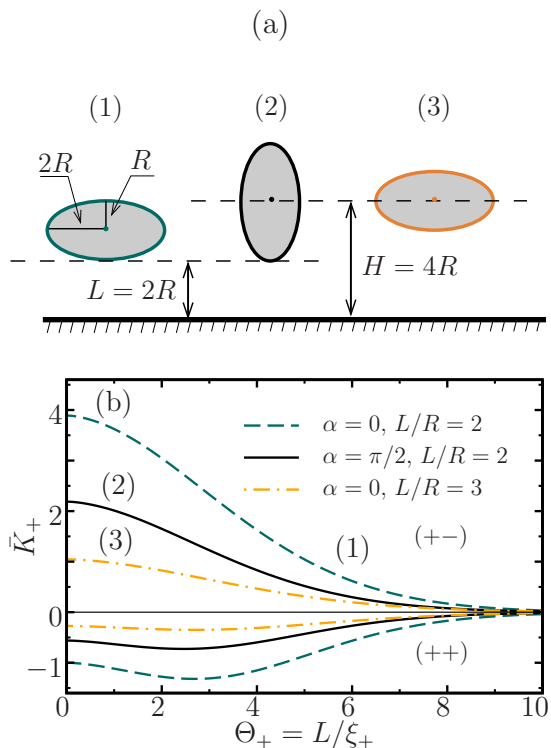


FIG. 4: (color online) (a) Comparison between three ellipse configurations such that the configurations (1) and (2) have the same closest distance $L = 2R$, while configurations (2) and (3) have the same distance $H = 4R$ between the center of the particle and the wall. For the configuration (1) $H = 3R$ and for the configuration (3) $L = 3R$. (b) The universal scaling function $\bar{K}_+ = K_+(\Theta_+, \Delta, \alpha; \delta = 2)/|K_+(\Theta_+ = 0, \Delta = 2, \alpha = 0; \delta = 2)|$ as a function of the reduced temperature $\Theta_+ = L/\xi_+$ for an ellipse ($d = 2$). The dashed lines (1) represent the results for an ellipse oriented parallel to the wall ($\alpha = 0, L/R = 2, H/R = 3$) at the same closest distance between its surface and the wall as an ellipse which is oriented perpendicular to the wall ($\alpha = \pi/2, L/R = 2, H/R = 4$, solid lines (2)). The dash-dotted lines (3) represent the results for an ellipse oriented parallel to the wall ($\alpha = 0, L/R = 3, H/R = 4$) and at the same distance between its center of mass and the wall as compared to the ellipse which is oriented perpendicular to the wall (solid lines (2)). The positive (negative) curves correspond to $+ -$ ($++$) boundary conditions on the ellipse and at the wall. The force is expressed in units of the absolute value of the Casimir force for $\alpha = 0$ and $\Delta = L/R = 2$ at the critical point ($\Theta_+ = 0$) and for $++$ boundary conditions.

note that the Derjaguin approximation underestimates the strength of the force for $\alpha = \pi/2$ and overestimates it for $\alpha = 0$.

For the comparison of the Casimir force acting on ellipsoids with various orientations and at a fixed distance from the wall in z -direction, there are two interesting choices for this distance: The closest distance L between the wall and the surface of the ellipsoid, and the distance H between the center of the ellipsoid and the wall (see

Fig. 1). Figure 4(b) displays the corresponding scaling function for an ellipse ($d = 2$) which is oriented perpendicular to the wall ($\alpha = \pi/2, L/R = 2, H/R = 4$, solid lines; (2) in Fig. 4) together with the scaling function for an ellipse which is oriented parallel to the wall at the same distance L ($\alpha = 0, L/R = 2, H/R = 3$, dashed lines; (1) in Fig. 4) and the scaling function for an ellipse which is oriented parallel to the wall at the same distance H ($\alpha = 0, L/R = 3, H/R = 4$, dash-dotted lines; (3) in Fig. 4). If the ellipse is orientated perpendicular to the wall (solid lines), the magnitude of the Casimir force is smaller than if the ellipse is parallel to the wall at the same closest distance between the wall and the surface of the ellipse (dashed lines). Compared to an ellipse which is parallel to the wall at the same distance between the center of the ellipse and the wall (dash-dotted lines) the magnitude of the Casimir force acting on the perpendicular oriented ellipse is larger (solid lines). We have confirmed numerically that these relations between the strengths of the fluctuation induced forces are valid for arbitrary values of $\Delta = L/R$ including the limits $\Delta \rightarrow 0$ and $\Delta \gg 1$. In the latter limit these results are in agreement with the predictions of a small particle operator expansion [68] which can be used near the critical point ($\Theta_+ \rightarrow 0$) as long as all semi-axes of the ellipse are much smaller than all other lengths such as the correlation length or the distance between the surface of the particle and the wall.

In Fig. 5 the scaling function K_+ with a suitable normalization is plotted as a function of the angle α between the main axis of the spheroid and the wall (see Fig. 1) for a fixed rescaled minimal distance $L/\xi_+ = \text{const}$. As expected, the force is larger for more elongated colloids (R_d/R_1 large) but only for small α (i.e., if the colloids are almost parallel to the wall). If the colloids are tilted more towards the perpendicular orientation ($\alpha \gtrsim 30^\circ$), the opposite trend is observed. As discussed at the beginning of this subsection, this is due to the shapes of the prolate spheroids: for the perpendicular orientation $G_{\text{spheroid}}^{-1/2}(\alpha = \pi/2) = R^2/R_d$ for $d = 3$ and $G_{\text{ellipse}}^{-1/2}(\pi/2) = R/R_d^{1/2}$ for $d = 2$, which decrease upon increasing R_d , whereas for the parallel orientation one has $G_{\text{spheroid}}^{-1/2}(0) = R_d$ for $d = 3$ and $G_{\text{ellipse}}^{-1/2}(0) = R_d/R^{1/2}$ for $d = 2$ which increase upon increasing R_d . The scaling functions for the hypercylinders \mathcal{K}_3 (Fig. 5(a)) and \mathcal{K}_2 (Fig. 5(b)) are rather similar.

C. Casimir torque

The torque scaling function M_+ (see Eqs. (3), (14), and (15)) as a function of the angle α (Fig. 1) between the main axis of an elongated colloid and the wall is presented in Fig. 6 for both $++$ and $+ -$ boundary conditions and for a fixed rescaled minimal distance $L/\xi_+ = \text{const}$ with the pivot point $\mathbf{r}^{(1)}$ (see Eq. (15)) taken to be the point closest to the wall (denoted as a circle in Fig. 1). The scaling function is positive for $++$ and negative for $+ -$

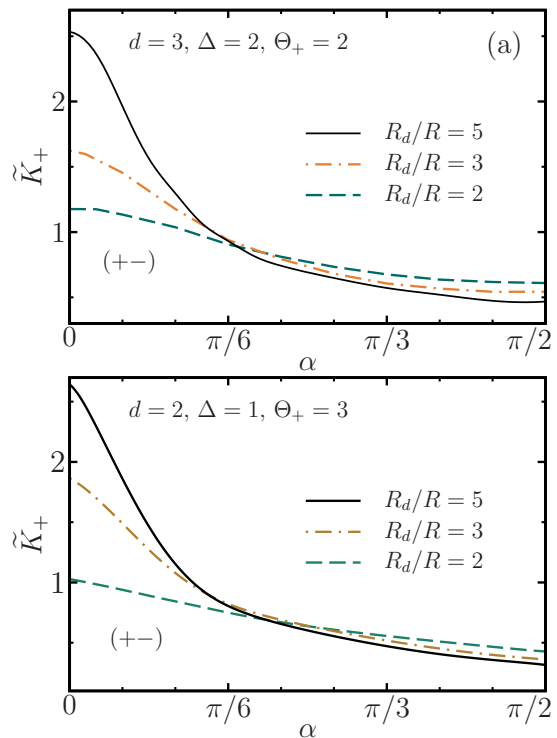


FIG. 5: (color online) The universal scaling function $\tilde{K}_+ = K_+(\Theta_+, \Delta, \alpha; \delta)/K_+(\Theta_+ = 0, \Delta; \delta = 1)$ for $+ -$ boundary conditions as a function of the angle α between the main axis of the spheroid and the wall (see Fig. 1) for three values of the ratio $\delta = R_d/R$. In (a) $d = 3, \Theta_+ = L/\xi_+ = 2$, and $\Delta = L/R = 2$, while in (b) $d = 2, \Theta_+ = 3$, and $\Delta = 1$. The force is expressed in terms of the Casimir force at the critical point for $+ -$ boundary conditions for a sphere ($d = 3$) with radius $R = R_1 = L/2$ in (a) and for a disk ($d = 2$) with radius $R = L$ in (b). All curves correspond to keeping temperature and the *minimal distance* L fixed upon varying the orientation (see Fig. 1).

boundary conditions. This means that in the $++$ case the configuration is optimal (i.e., the free energy is lowest) if the colloid is parallel ($\alpha = 0$) while in the $+ -$ case if it is perpendicular to the wall ($\alpha = \pi/2$). As one may expect, the torque vanishes for $\alpha = 0$ and $\alpha = \pi/2$, which for $+ -$ ($++$) boundary conditions correspond to a maximum (minimum) and a minimum (maximum) of the free energy, respectively. Also as expected, the magnitude of the torque increases upon increasing the ratio R_d/R_1 (for fixed R_1/L).

As we have already mentioned, one can introduce different pivots with respect to which the torque is exerted on the ellipsoid, such as the point of closest approach to the wall (denoted as a circle in Fig. 1) and the center of the ellipsoid (denoted as a square in Fig. 1). The latter is more convenient to use if the ellipsoid is far from the substrate. In this case the motion of the ellipsoid can be described in terms of its center of mass (which we assume to coincide with the geometrical center); accordingly the

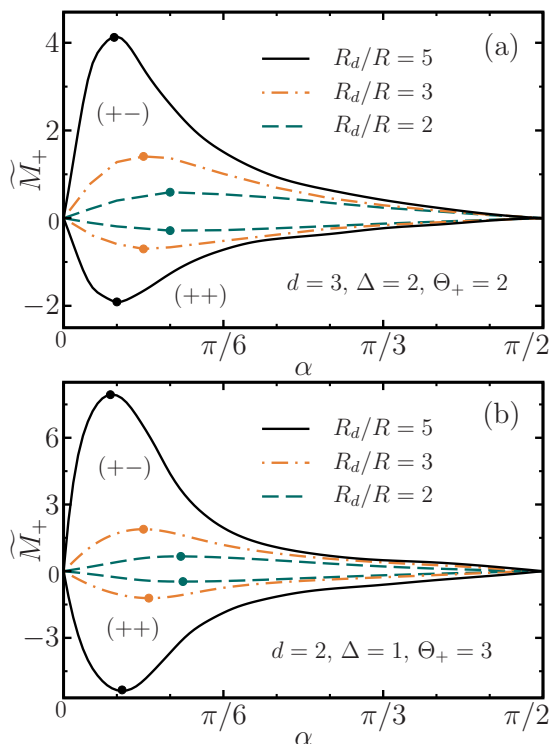


FIG. 6: (color online) The universal torque scaling function $\widetilde{M}_+ = M_+(\Theta_+, \Delta, \alpha; \delta) / |K_+(\Theta_+ = 0, \Delta; \delta = 1)|$ as a function of the angle α between the wall and the main axis of an elongated colloid (Fig. 1) for three values of the ratio $\delta = R_d/R$. In (a) $d = 3$, $\Delta = L/R = 2$, and $\Theta_+ = L/\xi_+ = 2$, while in (b) $d = 2$, $\Delta = 1$, and $\Theta_+ = 3$. The positive (negative) curves correspond to $+-$ ($++$) boundary conditions. $\widetilde{M}_+ > 0$ ($\widetilde{M}_+ < 0$) implies that the torque acts as to increase (decrease) α . The torque is expressed in terms of the absolute value of the Casimir force for $++$ boundary conditions at the critical point for a ($d = 3$)-sphere with radius $R = R_1 = L/2$ in (a) and for a disk ($d = 2$) with radius $R = L$ in (b). The extrema are marked by full dots; their positions shift to smaller values of α upon increasing R_d/R . All curves correspond to keeping temperature and the *minimal distance* L fixed upon varying the orientation, and the pivot is taken to be the point closest to the wall (denoted as a circle in Fig. 1).

orientational degrees of freedom of the ellipsoid should consistently be described also with respect to the center of the ellipsoid. If the ellipsoid is sufficiently close to the substrate, it is more convenient to monitor the orientations of the ellipsoid with respect to the point of closest approach to the wall. One reason is that in the region close to the substrate not all orientations of the ellipsoid with respect to its center of mass are allowed because the particle cannot penetrate the substrate (c.f., Sec. IV and Fig. 8(a)). One can also imagine that the ellipsoid is trapped in a relatively shallow potential well of optical tweezers. In this situation the rotation of the ellipsoidal particle occurs naturally with respect to the point closest to the wall.

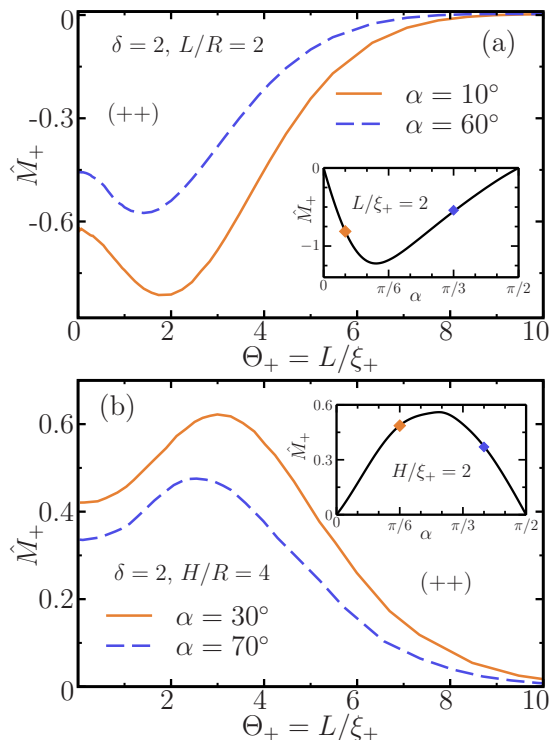


FIG. 7: (color online) The universal torque scaling function $\hat{M}_+ = M_+(\Theta_+, \Delta, \alpha; \delta = 2) / K_+^{(II)}(\Theta_+ = 0)$ as a function of temperature for a spheroid (spheroido-cylinder $\mathcal{K}_{d=3}$ in $D > d$) with $\delta = R_d/R = 2$ for $++$ boundary conditions and for two values of the angle α between the main axis of the spheroid and the wall (Fig. 1). In (a) the *surface-to-surface* distance L is fixed with $\Delta = L/R = 2$ and the torque is calculated with respect to the point of closest approach (denoted as a circle in Fig. 1). In (b) the distance H between the wall and the *center of the ellipsoid* is fixed with $H/R = 4$ and the torque is calculated with respect to the center of the ellipsoid (denoted as a square in Fig. 1). The insets show \hat{M}_+ as a function of α for $L/\xi_+ = 2 = \text{const}$ in (a) and $H/\xi_+ = 2 = \text{const}$ in (b). The symbols in the insets correspond to the values of the angle α represented in the main plots. The torque is expressed in term of the absolute value of the Casimir force for $++$ boundary conditions at the critical point for the film geometry. In both (a) and (b) the torque is strongest at a distinct temperature above (and not at) T_c .

In Figs. 7(a) and 7(b) the torque scaling function M_+ with a suitable normalization is plotted for these two choices of the pivot for a few values of the angle α between the main axis of the ellipsoid and the wall and for $++$ boundary conditions. In Fig. 7(a) the torque is calculated with respect to the point closest to the wall, and consistently we consider a constant minimal rescaled distance $L/\xi_+ = \text{const}$ for all angles. In Fig. 7(b) the torque is calculated with respect to the center of the ellipsoid, so that the rescaled distance between the center of the ellipsoid and the wall is fixed, i.e., $H/\xi_+ = \text{const}$. Note that the scaling function is negative in the former and positive in the latter case. This means that if the

surface-to-surface distance L is kept fixed (for instance, by optical tweezers or by the wall), the optimal configuration of an ellipsoidal colloid is to be parallel to the wall ($\alpha = 0$). However, if the ellipsoid rotates with respect to its center of mass, the optimal configuration is to be perpendicular to the wall ($\alpha = \pi/2$). In the $+ -$ case the situation is reverse.

IV. COMPARISON WITH THE QUANTUM-ELECTRODYNAMIC CASIMIR INTERACTION AND THE POLYMER INDUCED DEPLETION INTERACTION

The quantum-electrodynamic Casimir interaction [43, 44] and the polymer induced depletion interaction [46, 47, 48, 49] lead to pronounced effects on the orientational ordering of non-spherical particles, too. The schematic presentation in Fig. 8 illustrates the influence of these two interactions and of the critical Casimir interaction on the orientation of a prolate ellipsoidal particle near a planar wall. For the purpose of the discussion, the region adjacent to the wall can be divided into three sub-regions denoted as I, II, and III (see Fig. 8). In region I not all orientations of the prolate ellipsoid are allowed because the particle cannot penetrate the wall. In the case of an attractive critical Casimir interaction the prolate ellipsoid reaches its most favorable configuration of lying parallel to the wall by tilting such that for a prescribed distance of its center from the wall its optimum angle in region I is the one for which it is in touch with the wall (Fig. 8(a)). The influence of both the quantum-electrodynamic Casimir interaction and the polymer induced depletion interaction on the orientation of an ellipsoid in region I has not yet been studied. For larger distances from the wall, in regions II and III, the critical Casimir torque drives the prolate ellipsoid into an orientation perpendicular to the wall (Fig. 8(a)). In the case of the quantum-electrodynamic Casimir interaction and of the polymer induced depletion interaction the preferred orientation in region II is perpendicular [44] (Fig. 8(b)) and parallel [46, 48, 49] (Fig. 8(c)) to the wall, respectively. Upon further increasing the distance from the wall a change of the preferred orientation has been found in the case of a scalar model of quantum-electrodynamics with Neumann boundary conditions both at the surface of the particle and at the wall [44] (Fig. 8(b)) and in the case of ideal polymers acting as depletion agents [46] (Fig. 8(c)).

The polymer induced depletion interaction has been calculated [46, 48, 49] in the so-called protein limit in which the size of the ellipsoid is small compared to the polymer size characterized by the radius of gyration. By using the small particle operator expansion, it has been shown that the extension of region II along the z -direction is given by the radius of gyration of the polymers acting as depletion agents [46, 47, 48, 49]. However, the presently available non-spherical colloidal particles

are larger than typical polymers and monitoring small particles by optical techniques is very difficult. Therefore, it would be rewarding to study theoretically and experimentally the polymer induced depletion interaction beyond the small particle limit.

We emphasize that the preferred orientations of a prolate ellipsoid due to the quantum-electrodynamic Casimir interaction (Fig. 8(b)) have been obtained by considering a *scalar* model instead of the actual vectorial electromagnetism. In the actual case of the electromagnetic field, which implies Dirichlet boundary conditions, and a slightly deformed sphere, the preferred orientation of a prolate ellipsoid is the one perpendicular to the wall in both regions II and III [44]. Future work in this area may focus on the understanding of the influence of the quantum-electrodynamic Casimir interaction on ellipsoids of arbitrary eccentricities and at small distances from the wall.

V. CONCLUSIONS

We have investigated the critical Casimir effect for single non-spherical colloidal particles immersed in a fluid near its critical point and exposed to a laterally homogeneous planar wall. For an ellipsoidal colloidal particle the resulting critical Casimir force and torque can be characterized by universal scaling functions K_{\pm} (Eq. (1)) and M_{\pm} (Eq. (3)), respectively, which depend on the dimensionless scaling variables $\Theta_{\pm} = L/\xi_{\pm}$, $\Delta = L/R_1$, the angle α between the main axis of the ellipsoid and the wall, and the ratios $\delta_{i-1} = R_i/R_1$, where R_1 is the smallest semi-axis of the ellipsoid, R_i ($i = 2, \dots, d$) are $d - 1$ remaining semi-axes, L is the closest distance between the surface of the ellipsoid and the wall (see Fig. 1), and ξ_{\pm} is the bulk correlation length above (+) and below (-) the critical point. The scaling functions have been calculated within mean-field theory, which represents the leading order term in a systematic $\epsilon = 4 - D$ expansion. The dependence of the scaling functions K_{\pm} on the scaling variable Θ_{\pm} exhibits behaviors which are qualitatively similar to those of a spherical colloidal particle (see Figs. 2 and 3). The strength of the force depends on the orientation of the colloidal particle relative to the wall: for elongated colloids it is stronger if the colloid is oriented parallel to the wall at the same surface-to-surface distance L (see Figs. 4 and 5). If ellipsoidal colloids are oriented perpendicular to the wall, the force is stronger for shorter colloids (see Fig. 5). We note, however, that the latter effect is due to the specific shape of the ellipsoid at its elongated edge (see Subsec. III B), while the former effect is more general.

The sign of the universal torque scaling function M_{+} depends on the boundary conditions and on the pivot with respect to which the particle rotates. Thus, if the pivot is chosen to be the point on the particle surface closest to the wall (denoted as a circle in Fig. 1), the scaling function is positive for equal ($++$) and negative

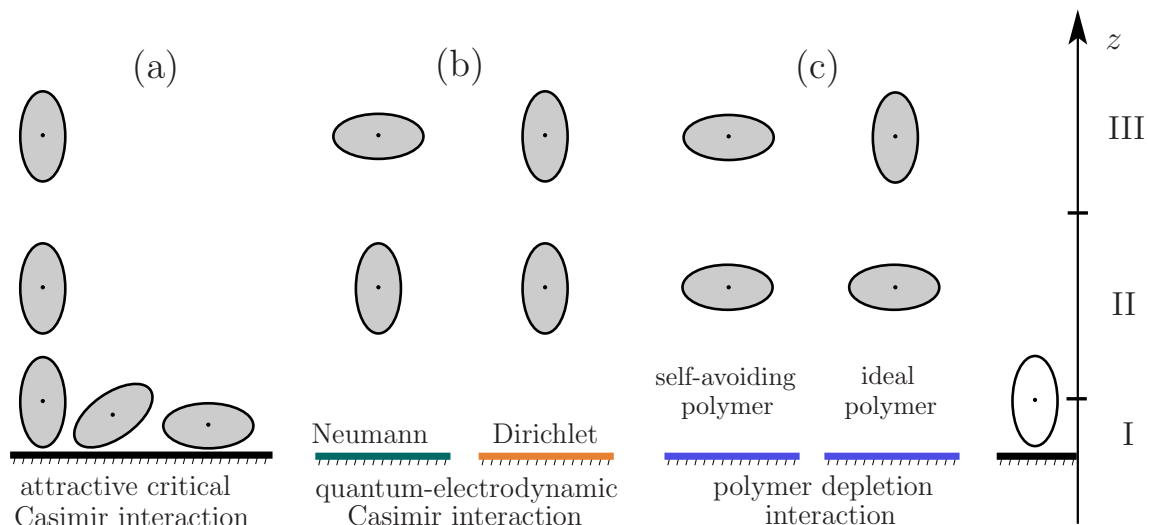


FIG. 8: (color online) Illustration of the preferred orientation of a prolate ellipsoid at a fixed distance of its center from a planar wall in the z -direction. Only the projection onto the plane of the figure is shown. The centers of the ellipsoids are chosen to lie within the plane of the figure. (a) In the case of the attractive critical Casimir interaction the ellipsoid is oriented perpendicular to the wall in regions II and III, while it prefers to touch the wall in region I because in that configuration the corresponding Casimir force is stronger than for other orientations. (b) In the case of a scalar model of quantum-electrodynamics and for Neumann boundary conditions on the surface of the ellipsoid, a change of the preferred orientation has been found for Neumann boundary conditions at the wall [44]. For Neumann boundary conditions on the particle surface and Dirichlet boundary conditions at the wall the energy is minimal if the ellipsoid is perpendicular to the wall in both regions II and III. In the case of mixed Dirichlet and Neumann boundary conditions the quantum-electrodynamic Casimir force is repulsive. (c) Using the small particle operator expansion it has been shown that the attractive polymer induced depletion interaction leads to a change of the preferred orientation of the ellipsoid in the case of the ideal polymers, while the favorable orientation is the parallel one in both regions II and III in the case of self-avoiding polymers [46, 48, 49]. The preferred orientation of an ellipsoidal particle in region I has not yet been studied for the quantum-electrodynamic Casimir force or the polymer depletion induced interactions. The extension of region II in the z -direction is of the order of the length of the long axis of the ellipsoid in (b) and given by the radius of gyration of the polymers in (c).

for opposing ($+ -$) boundary conditions at the wall and at the particle surface (see Figs. 6 and Fig. 7(a)). This means that *at the same closest distance* L between the surfaces of the colloid and the wall an elongated particle tends to orient itself parallel to the wall for equal boundary conditions and perpendicular to the wall for opposing boundary conditions. We expect this situation to be realized if a particle is close to the wall or, for instance, if it is trapped by optical tweezers. An opposite effect is observed if the center of the particle is kept fixed (see Fig. 7(b)). In this case an elongated colloid prefers an orientation perpendicular to the wall for equal boundary conditions and parallel to the wall for opposing boundary

conditions. It is worthwhile to note that this conclusion agrees qualitatively with the asymptotic results obtained from the small-particle operator expansion [68] (see also Fig. 8(a)).

Acknowledgments

S. K. and L. H. gratefully acknowledge support by grant HA 2935/4-1 of the Deutsche Forschungsgemeinschaft.

-
- [1] M. E. Fisher and P. de Gennes, C. R. Acad. Sci. Paris B **287**, 207 (1978).
 [2] M. Krech, *The Casimir Effect in Critical Systems* (World Scientific, Singapore, 1994).
 [3] J. Brankov, D. M. Danchev, and N. S. Tonchev, *Theory of Critical Phenomena in Finite-Size Systems* (World Scientific, Singapore, 2000).

- [4] H. B. G. Casimir, Proc. K. Ned. Akad. Wet. **51**, 793 (1948).
 [5] M. Kardar and R. Golestanian, Rev. Mod. Phys. **71**, 1233 (1999).
 [6] M. Krech and S. Dietrich, Phys. Rev. Lett. **66**, 345 (1991).
 [7] M. Krech and S. Dietrich, Phys. Rev. A **46**, 1886 (1992).

- [8] M. Krech and S. Dietrich, Phys. Rev. A **46**, 1922 (1992).
- [9] R. Evans and J. Stecki, Phys. Rev. B **49**, 8842 (1994).
- [10] M. Krech, Phys. Rev. E **56**, 1642 (1997).
- [11] B. M. Law, Prog. Surf. Sci. **66**, 159 (2001).
- [12] O. Vasilyev, A. Gambassi, A. Maciolek, and S. Dietrich, Europhys. Lett. **80**, 60009 (2007).
- [13] A. Maciolek and S. Dietrich, Europhys. Lett. **74**, 22 (2006).
- [14] A. Maciolek, A. Gambassi, and S. Dietrich, Phys. Rev. E **76**, 031124 (2007).
- [15] D. Dantchev, F. Schlesener, and S. Dietrich, Phys. Rev. E **76**, 011121 (2007).
- [16] A. Hucht, Phys. Rev. Lett. **99**, 185301 (2007).
- [17] D. Grüneberg and H. W. Diehl, Phys. Rev. B **77**, 115409 (2008).
- [18] M. Sprenger, F. Schlesener, and S. Dietrich, J. Chem. Phys. **124**, 134703 (2006).
- [19] M. Tröndle, L. Harnau, and S. Dietrich, J. Chem. Phys. **129**, 124716 (2008).
- [20] E. Eisenriegler and U. Ritschel, Phys. Rev. B **51**, 13717 (1995).
- [21] T. W. Burkhardt and E. Eisenriegler, Phys. Rev. Lett. **74**, 3189 (1995).
- [22] A. Hanke, F. Schlesener, E. Eisenriegler, and S. Dietrich, Phys. Rev. Lett. **81**, 1885 (1998).
- [23] F. Schlesener, A. Hanke, and S. Dietrich, J. Stat. Phys. **110**, 981 (2003).
- [24] R. Garcia and M. H. W. Chan, Phys. Rev. Lett. **83**, 1187 (1999).
- [25] R. Garcia and M. H. W. Chan, Phys. Rev. Lett. **88**, 086101 (2002).
- [26] A. Ganshin, S. Scheidemantel, R. Garcia, and M. H. W. Chan, Phys. Rev. Lett. **97**, 075301 (2006).
- [27] M. Fukuto, Y. F. Yano, and P. S. Pershan, Phys. Rev. Lett. **94**, 135702 (2005).
- [28] S. Rafai, D. Bonn, and J. Meunier, Physica A **386**, 31 (2007).
- [29] P. de Gennes, C. R. Acad. Sci. Ser. II **292**, 701 (1981).
- [30] D. Beysens and D. Estève, Phys. Rev. Lett. **54**, 2123 (1985).
- [31] P. D. Gallagher and J. V. Maher, Phys. Rev. A **46**, 2012 (1992).
- [32] P. D. Gallagher, M. L. Kurnaz, and J. V. Maher, Phys. Rev. A **46**, 7750 (1992).
- [33] M. L. Kurnaz and J. V. Maher, Phys. Rev. E **51**, 5916 (1995).
- [34] D. Beysens, J.-M. Petit, T. Narayanan, A. Kumar, M. L. Broide, and D. Estève, Ber. Bunsenges. Phys. Chem. **98**, 382 (1994).
- [35] T. Narayanan, A. Kumar, E. S. R. Gopal, D. Beysens, P. Guenoun, and G. Zalczer, Phys. Rev. E **48**, 1989 (1993).
- [36] Y. Jayalakshmi and E. W. Kaler, Phys. Rev. Lett. **78**, 1379 (1997).
- [37] H. Gröll and D. Woermann, Ber. Bunsenges. Phys. Chem. **101**, 814 (1997).
- [38] H. Guo, T. Narayanan, M. Sztuchi, P. Schall, and G. H. Wegdam, Phys. Rev. Lett. **100**, 188303 (2008).
- [39] C. Hertlein, L. Helden, A. Gambassi, S. Dietrich, and C. Bechinger, Nature **451**, 172 (2008).
- [40] F. Soyka, O. Zvyagolskaya, C. Hertlein, L. Helden, and C. Bechinger, Phys. Rev. Lett. **101**, 208301 (2008).
- [41] M. Tröndle, S. Kondrat, A. Gambassi, L. Harnau, and S. Dietrich (2009), arXiv:0903.2113.
- [42] S. Kondrat, L. Harnau, and S. Dietrich, J. Chem. Phys. **126**, 174902 (2007).
- [43] A. W. Rodriguez, J. N. Munday, J. D. Joannopoulos, F. Capasso, D. A. R. Dalvit, and S. G. Johnson, Phys. Rev. Lett. **101**, 190404 (2008).
- [44] T. Emig, N. Graham, R. L. Jaffe, and M. Kardar (2008), arXiv:0811.1597v1.
- [45] G. Palágyi and S. Dietrich, Phys. Rev. E **70**, 046114 (2004).
- [46] E. Eisenriegler, A. Bringer, and R. Maassen, J. Chem. Phys. **118**, 8093 (2003).
- [47] E. Eisenriegler and A. Bringer, J. Phys.: Condens. Matter **17**, S1711 (2005).
- [48] E. Eisenriegler, J. Chem. Phys. **125**, 204903 (2006).
- [49] E. Eisenriegler, J. Chem. Phys. **124**, 144912 (2006).
- [50] L. Harnau and S. Dietrich, in *Soft Matter*, edited by G. Gompper and M. Schick (Wiley-VCH, 2007), vol. 3, p. 159.
- [51] Y. Liu, V. Abetz, and A. H. E. Müller, Macromolecules **36**, 7894 (2003).
- [52] C. H. M. Weber, A. Chiche, G. Krausch, S. Rosenfeldt, M. Ballauff, L. Harnau, and I. Göttker-Schnetmann, Nano Letters **7**, 2024 (2007).
- [53] P. M. Johnson, C. M. van Kats, and A. van Blaaderen, Langmuir **21**, 11510 (2005).
- [54] J.-W. Kim, R. J. Larson, and D. A. Weitz, J. Am. Chem. Soc. **128**, 14374 (2006).
- [55] S. Sacanna, L. Rossi, B. W. M. Kuipers, and A. P. Philipse, Langmuir **22**, 1822 (2006).
- [56] Y. Hu, J. Ge, T. Zhang, and Y. Yin, Adv. Mater. **20**, 4599 (2008).
- [57] M. Hoffmann, Y. Lu, M. Schrunner, M. Ballauff, and L. Harnau, J. Phys. Chem. B **112**, 14843 (2008).
- [58] K. Binder, in *Phase Transitions and Critical Phenomena*, edited by C. Domb and J. L. Lebowitz (Academic, London, 1983), vol. 8, p. 1.
- [59] H. W. Diehl, in *Phase Transitions and Critical Phenomena*, edited by C. Domb and J. L. Lebowitz (Academic, London, 1986), vol. 10, p. 75.
- [60] P. Hunter and A. Pullan, *FEM/BEM notes* (Department of Engineering Science, The University of Auckland, New Zealand, 2002).
- [61] J. Zinn-Justin, *Quantum Field Theory and Critical Phenomena* (Clarendon, 1989).
- [62] C. G. Callan, S. Coleman, and R. Jackiw, Annals of Physics **59**, 42 (1970).
- [63] J. C. Collins, Phys. Rev. D **14**, 1965 (1976).
- [64] J. C. Collins, Phys. Rev. Lett. **36**, 1518 (1976).
- [65] L. S. Brown, Annals of Physics **126**, 135 (1980).
- [66] B. Derjaguin, Kolloid Z. **69**, 155 (1934).
- [67] B. Derjaguin, V. M. Muller, and Y. P. Toporov, J. Colloid Interface Sci. **53**, 314 (1975).
- [68] E. Eisenriegler, J. Chem. Phys. **121**, 3299 (2004).